CFD Based Performance Evaluation of Solar Air Heater by using Centerline Perforated Sine Wave Baffles

Sharma, Sachin
Department of Mechanical Engineering, SOAE

Maithani, Rajesh
Department of Mechanical Engineering, SOAE

Randip Kumar Das
Department of Mechanical Engineering, IIT(ISM)

https://doi.org/10.5109/7183368

出版情報：Evergreen. 11 (2), pp.862-871, 2024-06. 九州大学グリーンテクノロジー研究教育センター
バージョン：

CFD Based Performance Evaluation of Solar Air Heater by using Centerline Perforated Sine Wave Baffles

Sachin Sharma[1], Rajesh Maithani[1*], Randip Kumar Das[2]

[1]Department of Mechanical Engineering, SOAE, UPES, Dehradun, Uttarakhand, 248007, India.

[2]Department of Mechanical Engineering, IIT(ISM), Dhanbad 826004, Jharkhand, India.

*Author to whom correspondence should be addressed:

E-mail: rmaithani@ddn.upes.ac.in

(Received January 4, 2024; Revised March 6, 2024; Accepted April 3, 2024).

Abstract: An exhaustive computational fluid dynamics (CFD) analysis has been conducted to assess the performance of a solar air heater employing perforated sine wave baffles. The study focused on four crucial operating parameters: Reynolds number (Re), relative streamwise pitch (P_{sw}/e), angle of attack (α), and relative perforation diameter (d_{PD}/e). The parameter ranges considered are: Re=3000-18000 (6 values), P_{sw}/e=8-14 (4 values), $\alpha=10^0$-45^0(4 values) and d_{PD}/e=0.24-0.48 (4 values) while maintaining a constant aspect ratio (W/H) of 12 for the heater. Through meticulous evaluation, the optimal set of geometric parameters has been determined based on three performance-defining factors: Nusselt number (Nu_{pb}), friction factor (f_{pb}) and thermo hydraulic performance (η). The findings of this study showcased the enhancements in the heater's performance. The Nusselt number exhibited a 6.6-fold increase, while the friction factor experienced a substantial 8-fold augmentation. The significant improvement in Nusselt number (Nu_{pb}) attributed to the substantial boost in turbulence and the reduction of the viscous layer within the system. Consequently, the maximum thermo hydraulic performance achieved an impressive value of 3.9.

Keywords: Computational fluid dynamics; Heat Transfer; Perforation; Sine wave baffles

1. Introduction

To meet the constantly rising worldwide energy requirements, solar thermal systems are essential in completing the panorama of traditional energy supplies. These systems harness abundant solar energy and convert it into heat and mechanical work. Solar air heaters (SAHs)[1)] and solar water heaters (SWHs) [2) 3)]are the most used solar thermal systems. SAHs found their applicability widely because of varied temperature ranges. However, achieving high conversion efficiency remains a significant challenge due to various factors that impact their performance. The low heat conductivity of the used working fluids is one of the primary problems with SAHs. This restriction makes it more difficult for heat to go through the system efficiently, which wastes energy. Additionally, some working fluids have suboptimal heat-absorbing capacities, which further reduces the overall efficiency of the system. Another issue that plagues these systems is the formation of viscous layers or scaling on the heat-absorbing surfaces, which can lead to decreased heat transfer efficiency. Researchers have been actively working to address these problems and have proposed a variety of approaches, categorized into active, passive, and compound, each offering unique solutions to enhance solar thermal system performance, shown in Fig. 1. These approaches differ in terms of their reliance on external energy sources. Active approaches necessitate external energy sources to operate effectively. They often involve additional mechanical or electrical components to improve energy conversion and heat transfer within the system. While these methods can be highly effective, they come with the drawback of increased complexity and energy input requirements. In contrast, passive approaches have gained prominence due to their simplicity in design and operation. These methods do not rely on external power sources, making them more sustainable and cost-effective. Passive techniques focus on optimizing the system's inherent characteristics and natural processes, allowing them to harness solar energy efficiently without the need for active interventions. The key advantage of passive approaches lies in their ease of construction and use, making them more accessible to a broader range of applications. These methods leverage the inherent properties of materials and natural phenomena, such as convection, radiation, and conduction, to enhance energy capture and transfer without the complexity associated with active approaches. The compound approaches use any of the two or more active and passive approaches[4)].

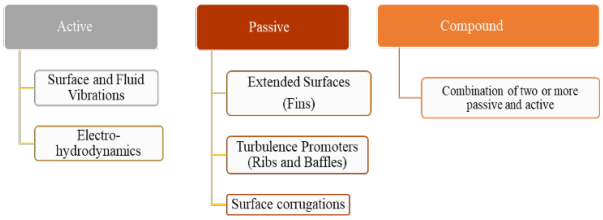

Fig.1: Active, Passive and Compound approaches.

In the realm of passive approaches, two key strategies have emerged for enhancing solar thermal systems: expanding the heat transfer area and incorporating turbulence enhancement, as depicted in Fig. 2. Recent research has emphasized the turbulence enhancement technique as a more sustainable solution, primarily because of its cost-effectiveness in terms of both initial setup and ongoing operation. However, it's important to acknowledge that this approach may incur higher operational costs owing to the increased demand for pumping power[5]. The most common turbulence promoters are ribs[6,7], baffles[8], winglets[9], protrusions[10] etc.

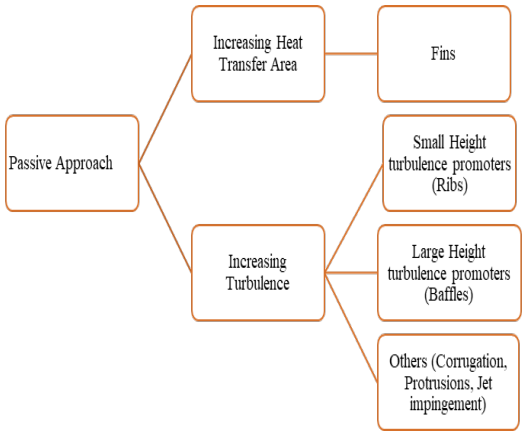

Fig. 2: Passive approaches.

2. Literature review

Ribs and baffles of several shapes have been used to promote solar air heater efficiency (SAHs). Among the commonly utilized ribs[11–15] and baffle designs are transverse[16], inclined transverse[17], S-shaped, sine-shaped[18][18–21], V-shaped[22], multiple V-shaped[23], and more[24–27][28–32][33–35]. In addition to these geometric variations, baffles have also been combined with fins and ribs[36–38] to further enhance SAH performance.

Kabeel et al.[39], performed experimental analysis on SAH by modifying the entrance of air. Baffled glazed blade was the modification. A total of nineteen fins were used and baffles were attached to the fins. The findings demonstrated that, at a given mass flow rate, the number of baffles directly affects SAH performance. Sarvanakumar et al.[40], used fins and baffles to analyze the exergetic performance of SAHs. The governing equations solved using MATLAB and results reflected the maximum exergy efficiency of 5.2% achieved at optimized states. Bensaci et al.[41], conducted experimental and numerical study to assess the performance of SAHs with varying baffle positions. The range of the Reynolds number was 2370–8430. The position of the baffles greatly influences the thermo-hydraulic performance of SAH, according to the data. Manjunath et al.[42], changed the SAH by utilising a corrugated absorber plate that is sinusoidal in shape. The performance was analyzed using CFD by adjusting the Reynolds number, wavelength, and aspect ratio. Overall, modified SAH's thermal efficiency increased by 12.5% when compared to smooth SAH. Skullong et al.[43], employed vortex generators of the winglet type in SAHs. In the investigation, generators that were trapezoidal and rectangular were employed. The findings showed that there was a significant increase in heat transfer because of the impinging jet produced by the vortex generators. Sahel et al.[44], employed perforated baffles to improve SAHs' thermal efficiency. Four holes were cut and positioned in three distinct orientations to create the perforation. The findings showed that the perforated baffles' pressure drop was twelve times smaller than that of the plain baffles with the same shape. Jain et al. [45], analyzed performance of SAH using V-Shaped perforated baffles. The results indicated that the perforated baffles resulted in 4.24- and 14.73-times augmentation of Nusselt number and friction factor respectively. Ghritlahre et al.[46] performed experiments to study the performance of SAH with arc shaped roughened SAH with apex up and down air flow. The results indicated that for the given mass flow rate the thermal performance of apex up is 6.9% more than apex down arrangements. Ghritlahre et al[47] further used different predictive models based on ANN and predicted the performance of SAH.

It is clear from the explanation above that using baffles greatly improves the efficiency of solar air heaters. But these baffles raise the friction factors, which raises the need for pumping power in the end. Conversely, allowing for perforation in the baffles enhances heat transfer and lowers the friction factor. The authors have examined the literature and found that no study has investigated how perforated sine wave baffles affect SAH performance. Because of this, the current study aims to investigate the heat transfer and friction characteristics of SAH with inline perforated sine wave baffles using Reynolds number (Re), relative streamwise pitch (P_{sw}/e), angle of attack (α), and perforation diameter (d_{PD}/e). The authors' work on employing sine wave baffles and their recommendation for perforation, particularly in the direction of principal flow, led to the decision to take an inline perforation in the baffles[18,21].

3. Computational Approach

In this work, the heater surface roughened by perforated sine wave baffles and smooth surface solar air heaters were compared in terms of performance using CFD analysis. ANSYS 19 R3 for academic use has been designed for modelling and simulation. The section below includes an appendix that details the process used for the computational analysis.

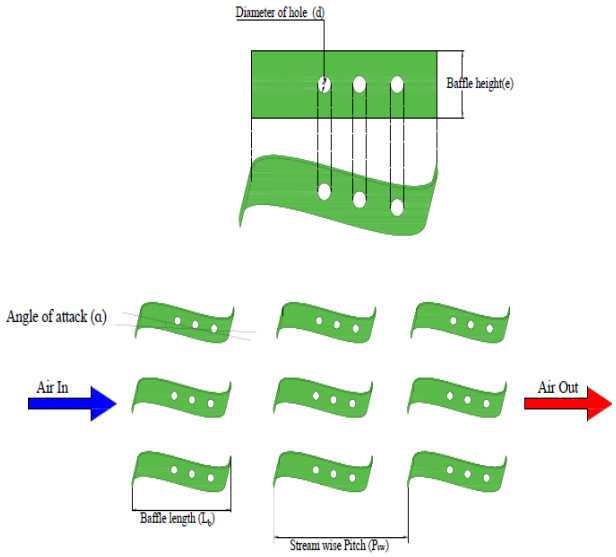

Fig. 3: Perforated sine wave baffles

Table 1. Operating and Geometrical parameters

S.No.	Parameter	Units & Range
Fixed		
1	Relative height (e/H)	0.5
2	Hydraulic Diameter (D_h)	46.12 mm
Geometric Parameters		
1	Relative stream wise pitch(P_{sw}/e)	8-14
2	Angle of attack (α)	0º-45º
3	Relative perforation diameter (d_{PD}/e)	0.24-0.48
3	Reynolds Number (Re)	3000-18000

3.1 Domain of Computations

The heater's computational domain is a rectangular channel with portions for the inlet, test, and exit. In accordance with ASHRAE guidelines, the intake and exit sections have maintained a minimum length. The apparent reason for keeping minimum lengths in the channel is to ensure the fully developed inside the channel[48]. The range of operating and geometric parameters are shown in Table 1. The schematic of various dimensions of all the sections are mentioned in Fig. 3.

3.2 Assumptions

During CFD analysis, the essential presumptions are:

1. The fluid flow is fully developed, turbulent, and three-dimensional.
2. The working fluid's physical properties are constant. The characteristics are calculated at the fluid's average temperature.
3. The fluid is incompressible.
4. The gravitational influence and body forces are insignificant.
5. At the walls, there are no-slip boundary conditions.
6. Natural convection is believed to have a minimal influence.

3.3 Boundary Conditions

Inlet, outlet, absorber, and adiabatic walls are the four boundaries that separate the fluid domain. At 300 K, the air attributes are measured [49]and are mentioned in Table 2. At the duct's inlet, the velocity admission condition is applied, and Re is used to compute the flow rate. The rate is between 0.944 and 5.661 m/sec. The no-slip boundary criterion is taken into consideration and the side walls are insulated. The absorber plate is assuming a 1000 W/m2 steady heat flow[50]. Though, the intensity of solar irradiation varies with geographical conditions and time of day. However, the average heat flux value has been taken as 1000 W/m^2 in numerous works [51,52]. The pressure outlet is determined by the conditions at the duct's exit. The schematic of all boundary conditions (BC) is shown in Fig. 4, and the values applied are mentioned in Table 3.

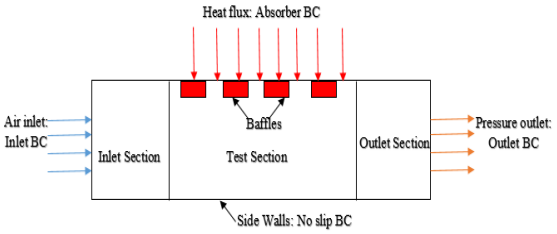

Fig. 4: Schematic of boundary conditions

Table 2. Properties of working fluid

Property	Value
Density(Kg/m^3)	1.165
Specific Heat (kJ /Kg K)	1.007
Thermal Conductivity (W/mK)	0.0258
Viscosity (Ns/m^2)	1.87×10^{-5}

Table 3. Boundary Conditions

S. No	Boundary Type	Condition	Values
1	Inlet	Velocity	Re = 3000 − 18000
		Temperature	300 K(fixed)
2	Outlet	Pressure	101325 Pa
3	Absorber	Heat Flux	1000 W/m^2
4	Side walls	No slip	Thermal Insulated

3.4 Governing Equations

The governing equations are appended below in Table 4

Table 4. Governing Equations

Name	Equation	Reference
Continuity	$\frac{D\rho}{Dt} + \rho(\nabla . V) = 0$	53)
Momentum	$\rho\frac{DV}{Dt} = \rho f - \nabla . p + \mu\nabla^2 V$	53)
Energy	$\rho\frac{DV}{Dt} = \frac{\partial Q}{\partial t} + k\nabla^2 T + \emptyset$	53)

3.5 Grid independencies test

The accuracy of computational results depends upon the meshing techniques, opted numerical scheme, and boundary conditions. Different meshing methods are available in the literature, which helps to get accurate results in minimum computational time. To make sure that the size of the grids has no bearing on the computing outcomes, the grid independence test has been carried out in this work. The Nu_{pb}. is computed with a fine, system-generated mesh for a constant Re of 10000. After that, the mesh was fine-tuned for the ensuing analysis, and Nu_{pb}. was once more computed using the identical Re. After 2707500 elements, the variation is less than 1 percent, according to observations. As a result, 2707500 items have been selected for in-depth analysis. The fluctuation of, Nu_{pb}. with the number of grid elements is seen in Table 5.

Table 5. Grid independence test

S.No	Number of Elements	Nusselt number (Nu_{pb})	% variations
1	950000	190.000	NA
2	1425000	194.446	2.34
3	1900000	198.121	1.89
4	2375000	200.340	1.12
5	2660000	202.203	0.93
6	2671400	203.558	0.67
7	2707500	203.700	0.07
8	2755000	203.802	0.05

The governing equations have been solved using the SIMPLE scheme, Renormalization-group (RNG) k–ε turbulence model with increased wall treatment. The order of 10^{-6} has been selected as the convergence range for the results.

3.6 Data Reduction

The pressure drops across the test section $(\Delta P)_d$, the temperature of the absorber plate (Tp), and the temperature of the air at the output surface (To) are considered as outlet parameters when modelling the SAH, while velocity (V_{avg}) is used as an input parameter. Re is utilised to calculate flow velocity. These output parameters are used to calculate the $Nu_{pb}$and f_{pb} as well as the η_{pb} . The collected computational results are analyzed using the equations mentioned below in Table 6.

3.7 CFD model validation

The computational results are validated by judging these results with standard equations and experimental results of Sharma et al.[55], which were obtained under similar operating conditions. The variations of the results are in Fig.5. The results of the Nusselt number (Nu_{ss}) are compared with the Dittus Boelter equation, and the friction factor (f_{ss}) results are compared with the Blasius Equation. The deviations of Nu_{ss} and f_{ss} results are 6.25% % and 7.10%, respectively.

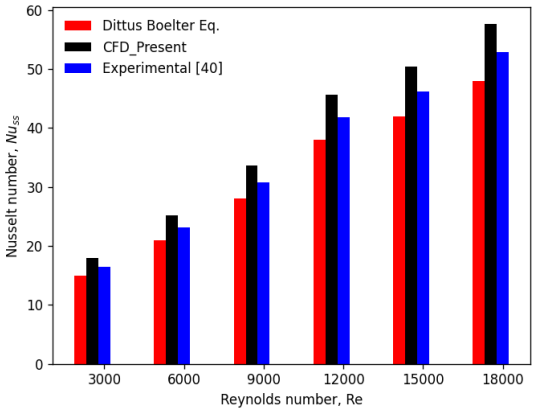

Fig. 5: Validation of CFD results

Table 6. Formulae used

Parameter	Symbol	Governing Equation	Ref.
Area of Absorber plate (m^2)	A_P	$W \times L$	
Hydraulic diameter (m)	D_h	$\frac{2(W \times H)}{(W + H)}$	56)
Air mass flow rate (Kg/sec)	$\dot{m}_a$	$C_d . A_o . \left[\frac{2 . \rho . (\Delta P)_o}{1 - \beta^4}\right]$	56)
Velocity of airflow(average) (m/sec)	V_{avg}	$\frac{m_a}{\rho W H}$	56)

Reynolds number	Re	$\frac{\rho V_{avg} D_h}{\mu}$	56)
Nusselt number	Nu	$\frac{hD_h}{k}$	56)
Friction factor	f	$\frac{2(\Delta P)_d D_h}{4\rho L V_{avg}^2}$	56)
Dittus Boelter equation	Nu_{ss}	$0.023 \times Re^{0.8} \times Pr^{0.4}$	57)
Blasius Equation	f_{ss}	$0.085 \times Re^{-0.25}$	58)
Thermohydraulic performance	η	$\frac{(Nu_{pb}/Nu_{ss})}{(f_{pb}/f_{ss})^{0.33}}$	59)

4. Results and discussions

This study explores the thermal characteristics of a solar air heater using CFD data obtained from simulations. The comparison of these simulation results with both theoretical frameworks and experimental evidence from prior research validates and substantiates the findings. The ensuing section comprehensively outlines and presents these confirmed results.

4.1 Effect of Perforation

The variations of Nusselt number (Nu_{pb}) by varying relative perforation diameter (d_{PD}/e) is shown in Fig.6(a); while the relative streamwise pitch (P_{sw}/e) and angle of attack (α) are fixed at 12 and 30^0, respectively. The measured results indicate that the increased order value of d_{PD}/e, the increases in the value of heat transfer. Based on Fig. 6(a), it can be observed that, Nu_{pb} rises as d_{PD}/e grows and reaches its maximum value atd_{PD}/e value of 0.40. Anticipatedly, in every scenario, the centerline jet perforated sine wave baffle wall generates a greater Nu_{pb} in comparison to the absence of a baffle wall. Because the top of the baffle creates subordinate stream jets, centerline jet perforated sine wave baffles perform better in terms of heat transmission. The cold fluid is carried by these subordinate jets' various rotating vortices from the central core area in the direction of the sine wave baffle walls. These subordinate flow jets disrupt boundary layer growth downstream of the reattachment zones, interfere with flow reattachment and recirculation among baffles, and interact with the mainstream.

The variations of friction factor (f_{pb}) by varying relative perforation diameter (d_{PD}/e). have been shown in Fig.6(b); while the relative streamwise pitch (P_{sw}/e) and angle of attack (α) are fixed at 12 and 30^0, respectively. One can note that f_{pb}. rises monotonically as P_{sw}/e grows. With a value of 0.48 for P_{sw}/e, the maximum value of f_{pb} has been observed. This is because the centerline jet perforated sine wave baffles help to increase turbulence stream jets, and due to this, reason increases the value of f_{pb} with increase P_{sw}/e. Figure 7 shows the airflow behaviour in centerline jet perforated sine wave baffles solar air heater.

4.2 Effect of angle of attack

Figure 8 shows the relationship between the $f_{pb}$and the Nu_{pb} as a function of the angle of attack as a function of the Re. (a-b). Increment in Re results in a rise in the Nu_{pb} and a decline in the f_{pb} for any given α. These figures show that the friction factor is maximum at $\alpha$of 30^0, while the Nu_{pb} is highest at 45^0. Additionally, the $Nu_{pb}$is nearly equal at 10^0, 20^0, and 45^0 attack angles. A plausible rationale could be that a larger angle of attack leads to a more notable pressure loss penalty throughout the test segment, but the heat transfer enhancement remains relatively same. As a result, as the angle of attack climbs above 45^0, the friction factor increases but the Nusselt number falls.

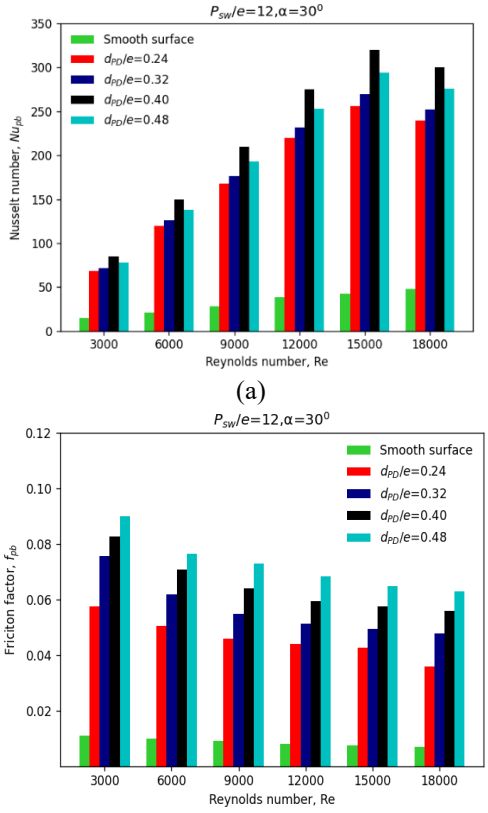

Fig. 6: Variations of (a) Nu_{pb} with d_{PD}/e (b) f_{pb} with d_{PD}/e

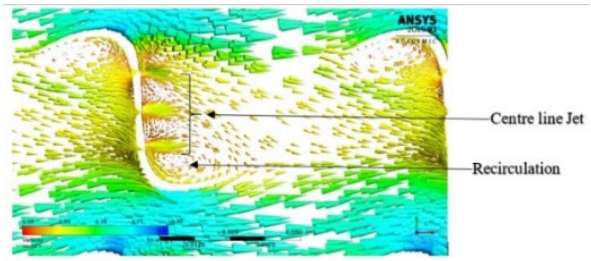

(a) Single baffle view at Re=9000)

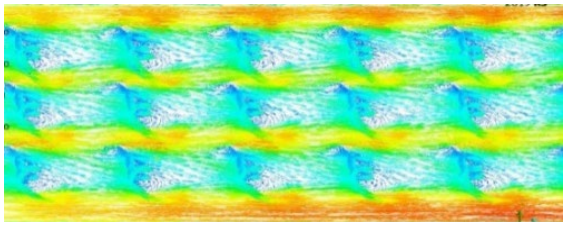

(b) Absorber plate at Re=12000

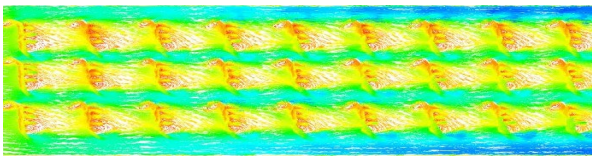

(c) Absorber plate at Re=15000

Fig. 7: Airflow behaviour at different *Re*.

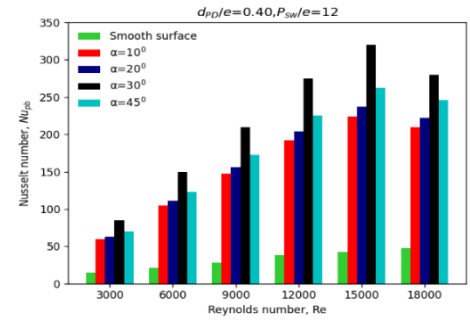

(a)

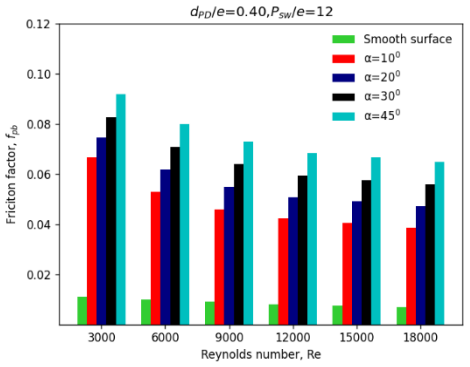

(b)

Fig. 8: Variations of (a) Nu_{pb} with α (b) f_{pb} with α

4.3 Effect of Pitch

The variations in the f_{pb} and the Nu_{pb} with P_{sw}/e are shown in Figs. 9(a) and (b). Figure. 9 provides a clear illustration of the maximum Nu_{pb} for perforated sine wave baffles at a P_{sw}/e of 12. (a). The Nu_{pb} value is still much greater than that of a perfectly smooth plate even at P_{sw}/e=8.0. The rate at which heat is transported from the absorber plate can be accelerated by raising the overall turbulence on the plate by increasing the number of baffles per unit length, even though flow reattachment might not happen at such a small pitch value. Pitch ratios cause the Nu_{pb} to peak at a value of 12. The flow seems to rejoin prior to the perforated sine wave baffles.

The improved heat transfer occurs for the same reasons as pitch ratios of 12. Still, the average Nusselt number values are significantly lower for pitch ratios of 14 because fewer perforated sine wave baffles elements are present per unit length of the absorber plate. Since more irregular perforated sine wave baffles parts per unit length of the absorber plate, the average Nusselt number continues to fall for a pitch ratio 14.

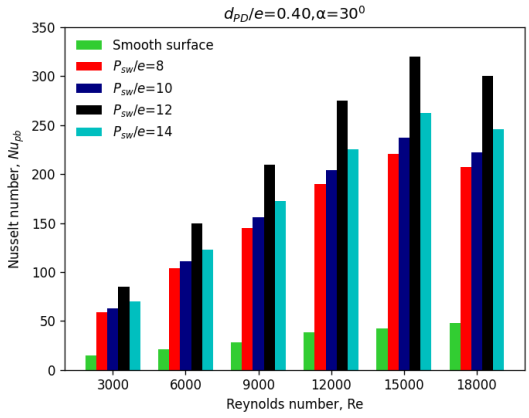

(a)

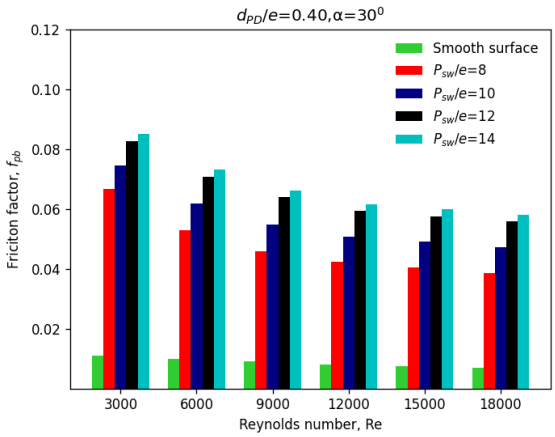

(b)

Fig. 9: Variations of (a) Nu_{pb} with P_{sw}/e (b) f_{pb} with P_{sw}/e

For pitch ratios of 12, there is a sudden increase in the Nu_{pb} that becomes more noticeable as the Re rises. Following reattachment, the flow picks up enough momentum to hit the perforated sine wave baffles first, creating substantial turbulence that speeds up heat transfer. It is believed that this pitch value will maximise the enhancement of heat transfer provided by the perforated sine wave baffles. Figure. 9 (b) shows how the relative roughness pitch affects the friction coefficient. There is

minimal friction because air flows through the perforated sine wave baffles at a pitch ratio of 8.0 without colliding with the absorber plate that sits between the upstream and downstream perforated sine wave baffles. When the pitch ratio is fourteen, the turbulence thus pierced.

4.4 Thermo-hydraulic performance

The current numerical investigation reveals that d_{PD}/e, α and P_{SW}/e have an evident influence on the thermo hydrodynamic performance of the centreline jet perforated sine wave baffles solar air heater. As per the above discussion, Nu_{pb} in jet-perforated sine wave baffles air channel improved with a significant rise in f_{pb}.

Figure 10(a-c) shows how several variable parameters, such as d_{PD}/e, α, and P_{SW}/e, affect the η in relation to Re. The overall performance parameter for various values of d_{PD}/e is shown in Fig. 10(a). It increases from 0.24 to 0.48 when the value of d_{PD}/e increases, and it decreases for all values of Re. It has been shown that η reaches its greatest value at d_{PD}/e=0.40. Because maximum heat transfer has been seen at d_{PD}/e=0.40 and the friction factor has not been at the greatest level, this value is the most appropriate to carry high heat transfer with little pumping power need. This is the reason for the highest η value. Similarly, the total performance parameter for various values of α is displayed in Fig. 10(b). It rose as the value of α climbed up to 30^0, and then it fell as the value of α increased further at all values of Re.

Figure 10(c) presents the overall performance parameter for a range of values of P_{SW}/e. The parameter increases from 8.0 to 12 as the value of P_{SW}/e increases, and it decreases for all values of Re. It has been observed that η reaches its highest value at P_{SW}/e = 12. This highest η value can be attributed to the fact that maximum heat transfer has been recorded at P_{SW}/e = 12, where the friction factor has not reached its highest level. This value is therefore the most appropriate to carry high heat transfer with little pumping power demand.

5. Conclusions

The key conclusions from the analysis of the data pertaining to the effects of perforation, flow attack angle, Reynolds number, and relative roughness pitch on the effectiveness of a flat plate solar air heater with perforated sine wave baffles are as follows:

- Relative perforation diameter (d_{PD}/e) value of 0.4 has been shown to be the maximum rise in the value of Nu_{pb}. On the other hand, the highest observed value of f_{Pb}. corresponds to relative perforation diameter value of 0.48.
- The greatest measured value of Nu_{pb} corresponds to a flow attack angle (α) value of 45^0, however the maximum value of, u_{pb}. has been seen at a flow attack angle (α) value of 30^0.
- At a relative roughness pitch (P_{SW}/e) value of 12, the maximum value of Nu_{Pb} has been seen. On the other hand, the highest observed value of Nu_{Pb}. corresponds to a relative roughness pitch value of 14.
- It has been determined that the ideal value of η is equal to $d_{pD}./e$ of 0.40, α of 30°, and P_{SW}/e of 12. The optimal value of η has been found to be 3.8 for Re of 9000.

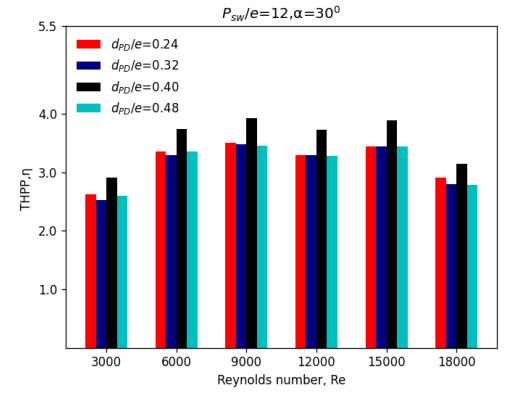

(a)

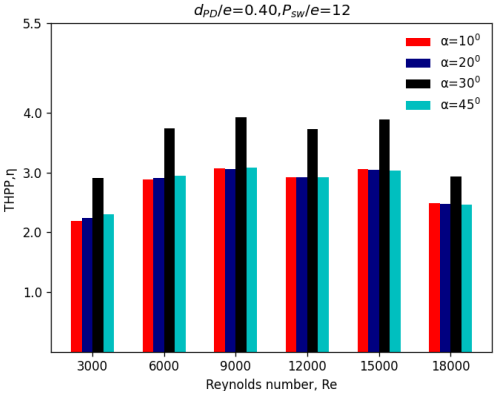

(b)

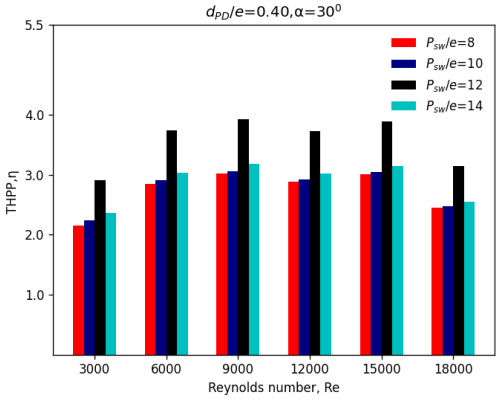

(c)

Fig. 10: Effect of various parameters on THPP

References

1) S. Zaphar, M. Chandrashekara, and G. Verma, "Thermal analysis of an evacuated tube solar collector using a one-end stainless steel manifold for

air heating applications under diverse operational conditions," *Evergreen*, 10 (*2*) 897–911 (2023). doi:10.5109/6792885

2) K. Tewari, and R. Dev, "Analysis of modified solar water heating system made of transparent tubes & insulated metal absorber," *Evergreen*, 5 (*1*) 62–72 (2018). doi:10.5109/1929731.
3) Y.D. Kim, K. Thu, and K.C. Ng, "Evaluation and parametric optimization of the thermal performance and cost effectiveness of active-indirect solar hot water plants," *Evergreen*, 2 (*2*) 50–60 (2015). doi:10.5109/1544080.
4) N. Kumar, M.K. Singh, V.S. Yadav, V. Singh, and A. Maheswari, "A comparative analysis of ribs and cans type solar air heater," *Evergreen*, 10 (*3*) 1449–1459 (2023). doi:10.5109/7151694.
5) R. Maithani, S. Sharma, and A. Kumar, "Thermo-hydraulic and exergy analysis of inclined impinging jets on absorber plate of solar air heater," *Renew Energy*, 179 84–95 (2021). doi:https://doi.org/10.1016/j.renene.2021.07.013.
6) R. Kumar, V. Goel, and A. Kumar, "Investigation of heat transfer augmentation and friction factor in triangular duct solar air heater due to forward facing chamfered rectangular ribs: a cfd based analysis," *Renew Energy*, 115 824–835 (2018). doi:https://doi.org/10.1016/j.renene.2017.09.010.
7) P. Promvonge, and C. Thianpong, "Thermal performance assessment of turbulent channel flows over different shaped ribs," *International Communications in Heat and Mass Transfer*, 35 (*10*) 1327–1334 (2008). doi:https://doi.org/10.1016/j.icheatmasstransfer.2008.07.016.
8) T. Saravanakumar, and D. Senthil Kumar, "Performance analysis on heat transfer characteristics of heat sink with baffles attachment," *International Journal of Thermal Sciences*, 142 (*March*) 14–19 (2019). doi:10.1016/j.ijthermalsci.2019.04.002.
9) R. Maithani, A. Kumar, M.A. Ali, N.K. Gupta, S. Sharma, T. Alam, S.M. Eldin, J.K. Bhutto, D. Dobrota, and F.C. Ciofu, "Exergy and sustainability analysis of a solar heat collector with wavy delta winglets as turbulent promoters: a numerical analysis," *Case Studies in Thermal Engineering*, 49 103293 (2023). doi:https://doi.org/10.1016/j.csite.2023.103293.
10) S. Yadav, and M. Kaushal, "ScienceDirect exergetic performance evaluation of solar air heater having arc shape oriented protrusions as roughness element," *Solar Energy*, 105 181–189 (2014). doi:10.1016/j.solener.2014.04.001.
11) Kumar, R. Maithani, A. Singh Yadav, and S. Sharma, "Effect of 450 protruded and dimpled rib height on the performance of triangular duct solar heat collector," *Mater Today Proc*, 63 253–258 (2022). doi:https://doi.org/10.1016/j.matpr.2022.03.044.
12) A.S. Yadav, A. Agrawal, A. Sharma, S. Sharma, R. Maithani, and A. Kumar, "Augmented artificially roughened solar air heaters," *Mater Today Proc*, 63 226–239 (2022). doi:10.1016/j.matpr.2022.02.548.
13) A.S. Yadav, O.P. Shukla, A. Sharma, and I.A. Khan, "CFD analysis of heat transfer performance of ribbed solar air heater," *Mater Today Proc*, 62 1413–1419 (2022). doi:https://doi.org/10.1016/j.matpr.2021.12.560.
14) A.S. Yadav, M.K. Dwivedi, A. Sharma, and V.K. Chouksey, "CFD based heat transfer correlation for ribbed solar air heater," *Mater Today Proc*, (2022). doi:https://doi.org/10.1016/j.matpr.2021.12.382.
15) A.S. Yadav, O.P. Shukla, A. Sharma, and I.A. Khan, "CFD analysis of heat transfer performance of ribbed solar air heater," *Mater Today Proc*, (2022). doi:https://doi.org/10.1016/j.matpr.2021.12.560.
16) A.J. Mahmood, "Experimental study of a solar air heater with a new arrangement of transverse longitudinal baffles," *J Sol Energy Eng*, 139 (*3*) (2017). doi:10.1115/1.4035756.
17) Varun, R.P. Saini, and S.K. Singal, "Investigation of thermal performance of solar air heater having roughness elements as a combination of inclined and transverse ribs on the absorber plate," *Renew Energy*, (2008). doi:10.1016/j.renene.2007.07.013.
18) S. Sharma, R.K. Das, and K. Kulkarni, "Parametric optimization of solar air heater having sine wave baffles as turbulators," *Experimental Heat Transfer*, 0 (*0*) 1–26 (2022). doi:10.1080/08916152.2022.2108525.
19) S. Sharma, R.K. Das, and K. Kulkarni, "Performance Evaluation of Solar Air Heater Using Sine Wave Shape Obstacle," in: S.K. Acharya, D.P. Mishra (Eds.), Current Advances in Mechanical Engineering, Springer Singapore, Singapore, 2021: pp. 541–553.
20) S. Sharma, R.K. Das, and K. Kulkarni, "Parametric optimization of solar air heater having sine wave baffles as turbulators," *Experimental Heat Transfer*, 00 (*00*) 1–26 (2022). doi:10.1080/08916152.2022.2108525.
21) S. Sharma, R.K. Das, and K. Kulkarni, "Experimental analysis and thermal management of solar air heater roughened with sine wave baffles," *Proceedings of the Institution of Mechanical Engineers, Part A: Journal of Power and Energy*, 236 (*7*) 1403–1417 (2022). doi:10.1177/09576509221092906.
22) P. Promvonge, and S. Skullong, "Enhanced thermal performance in tubular heat exchanger contained with v-shaped baffles," *Appl Therm Eng*, 185 (*August 2020*) 116307 (2021). doi:10.1016/j.applthermaleng.2020.116307.

23) R. Kumar, A. Kumar, R. Chauhan, and M. Sethi, "Heat transfer enhancement in solar air channel with broken multiple v-type baffle," *Case Studies in Thermal Engineering*, 8 187–197 (2016). doi:10.1016/j.csite.2016.07.001.
24) S. Sharma, R.K. Das, and K. Kulkarni, "Computational and experimental assessment of solar air heater roughened with six different baffles," *Case Studies in Thermal Engineering*, 27 101350 (2021). doi:https://doi.org/10.1016/j.csite.2021.101350.
25) P. Promvonge, and S. Skullong, "Thermal-hydraulic performance enhancement of solar receiver channel by flapped v-baffles," *Chemical Engineering Research and Design*, 182 87–97 (2022). doi:10.1016/j.cherd.2022.03.051.
26) N.T. Luan, and N.M. Phu, "Thermohydraulic correlations and exergy analysis of a solar air heater duct with inclined baffles," *Case Studies in Thermal Engineering*, 21 (*May*) 100672 (2020). doi:10.1016/j.csite.2020.100672.
27) B.K. Maheshwari, R. Karwa, and S.K. Gharai, "Performance study of solar air heater having absorber plate with half-perforated baffles," 2011 (2011). doi:10.5402/2011/634025.
28) Yaningsih, D. Danardono Dwi Prija Tjahjana, E. Prasetya Budiana, M. Muqoffa, Z. Arifin, K. Enoki, and T. Miyazaki, "Numerical study on the Effect of Rectangular and Triangular Counter-Rotating Vortex Generators on the H-Rotor Wind Turbine Performance," 2023.
29) V. Kumar Agrawal, and H.P. Khairnar, "Experimental & Analytical Investigation for Optimization of Disc Brake Heat Dissipation Using CFD," 2022.
30) S. Zaphar, and G. Verma, "Thermal Analysis of an Evacuated Tube Solar Collector using a One-end Stainless Steel Manifold for Air Heating Applications under Diverse Operational Conditions," 2023.
31) S. Kaushik, A. Kumar Verma, S. Singh, N. Kanojia, S. Panwar, S. Kindo, S. Uniyal, S. Goswami, D. Som, and N. Kumar Yadav, "Comparative Analysis of Fluid Flow Attributes in Rectangular Shape Micro Channel having External Rectangular Inserts with Hybrid Al 2 O 3 +ZnO+H 2 O Nano Fluid and (H 2 O) Base Fluid," 2023.
32) L.A. Rasheed, J. A-K Mohammed, and R.A. Jessam, "Performance Enhancement of a Single Pass Solar Air Heater by Adopting Wire Mesh Absorber Layer," 2023.
33) S. Chand, P. Chand, and H. Kumar Ghritlahre, "Thermal performance enhancement of solar air heater using louvered fins collector," *Solar Energy*, 239 10–24 (2022). doi:https://doi.org/10.1016/j.solener.2022.04.046.
34) H.K. Ghritlahre, M. Verma, J.S. Parihar, D.S. Mondloe, and S. Agrawal, "A detailed review of various types of solar air heaters performance," *Solar Energy*, 237 173–195 (2022). doi:https://doi.org/10.1016/j.solener.2022.03.042.
35) H.K. Ghritlahre, "Heat transfer and friction factor characteristic investigation of roughened solar air heater using arc-shaped wire rib roughness," *International Journal of Ambient Energy*, 43 (*1*) 5085–5099 (2022). doi:10.1080/01430750.2021.1934115.
36) H.S. Arunkumar, S. Kumar, and K.V. Karanth, "Analysis of a solar air heater for augmented thermohydraulic performance using helicoidal spring shaped fins-a numerical study," *Renew Energy*, 160 297–311 (2020). doi:10.1016/j.renene.2020.06.098.
37) E. Rahmani, T. Moradi, A. Fattahi, M. Delpisheh, and N. Karimi, "Numerical simulation of a solar air heater equipped with wavy and raccoon-shaped fins : the effect of fins ' height," *Sustainable Energy Technologies and Assessments*, 45 (*December 2020*) 101227 (2021). doi:10.1016/j.seta.2021.101227.
38) R. Kumar, and P. Chand, "Performance enhancement of solar air heater using herringbone corrugated fins," *Energy*, 127 271–279 (2017). doi:10.1016/j.energy.2017.03.128.
39) A.E. Kabeel, M.H. Hamed, Z.M. Omara, and A.W. Kandel, "On the performance of a baffled glazed-bladed entrance solar air heater," *Appl Therm Eng*, 139 (*May*) 367–375 (2018). doi:10.1016/j.applthermaleng.2018.04.141.
40) P.T. Saravanakumar, D. Somasundaram, and M.M. Matheswaran, "Exergetic investigation and optimization of arc shaped rib roughened solar air heater integrated with fins and baffles," *Appl Therm Eng*, 175 (*March*) 115316 (2020). doi:10.1016/j.applthermaleng.2020.115316.
41) C.E. Bensaci, A. Moummi, F.J. Sanchez de la Flor, E.A. Rodriguez Jara, A. Rincon-Casado, and A. Ruiz-Pardo, "Numerical and experimental study of the heat transfer and hydraulic performance of solar air heaters with different baffle positions," *Renew Energy*, 155 1231–1244 (2020). doi:10.1016/j.renene.2020.04.017.
42) M.S. Manjunath, K.V. Karanth, and N.Y. Sharma, "Numerical investigation on heat transfer enhancement of solar air heater using sinusoidal corrugations on absorber plate," *Int J Mech Sci*, 138–139 (*January*) 219–228 (2018). doi:10.1016/j.ijmecsci.2018.01.037.
43) S. Skullong, P. Promthaisong, P. Promvonge, C. Thianpong, and M. Pimsarn, "Thermal performance in solar air heater with perforated-winglet-type vortex generator," *Solar Energy*, 170 (*August 2017*) 1101–1117 (2018). doi:10.1016/j.solener.2018.05.093.

44) D. Sahel, H. Ameur, R. Benzeguir, and Y. Kamla, "Enhancement of heat transfer in a rectangular channel with perforated baffles," *Appl Therm Eng*, 101 156–164 (2016). doi:10.1016/j.applthermaleng.2016.02.136.
45) S.K. Jain, R. Misra, A. Kumar, and G. Das Agrawal, "Thermal performance investigation of a solar air heater having discrete v-shaped perforated baffles," *International Journal of Ambient Energy*, 43 (*1*) 243–251 (2022). doi:10.1080/01430750.2019.1636874.
46) H.K. Ghritlahre, P.K. Sahu, and S. Chand, "Thermal performance and heat transfer analysis of arc shaped roughened solar air heater – an experimental study," *Solar Energy*, 199 173–182 (2020). doi:https://doi.org/10.1016/j.solener.2020.01.068.
47) H.K. Ghritlahre, and R.K. Prasad, "Prediction of heat transfer of two different types of roughened solar air heater using artificial neural network technique," *Thermal Science and Engineering Progress*, 8 145–153 (2018). doi:https://doi.org/10.1016/j.tsep.2018.08.014.
48) S. Yadav, and R.P. Saini, "Numerical investigation on the performance of a solar air heater using jet impingement with absorber plate," *Solar Energy*, 208 (*July*) 236–248 (2020). doi:10.1016/j.solener.2020.07.088.
49) ANSYS, "ANSYS - turbulence modelling and the law of the wall: tutorial," *ANSYS User Manual*, 1–48 (2014).
50) V.B. Gawande, A.S.S. Dhoble, D.B.B. Zodpe, and S. Chamoli, "A review of cfd methodology used in literature for predicting thermo-hydraulic performance of a roughened solar air heater," *Renewable and Sustainable Energy Reviews*, 54 550–605 (2016). doi:10.1016/j.rser.2015.10.025.
51) A.S. Yadav, and J.L. Bhagoria, "A cfd (computational fl uid dynamics) based heat transfer and fl uid fl ow analysis of a solar air heater provided with circular transverse wire rib roughness on the absorber plate," *Energy*, 55 1127–1142 (2013). doi:10.1016/j.energy.2013.03.066.
52) K. Nidhul, S. Kumar, A.K. Yadav, and S. Anish, "Enhanced thermo-hydraulic performance in a v-ribbed triangular duct solar air heater: cfd and exergy analysis," *Energy*, 200 117448 (2020). doi:10.1016/j.energy.2020.117448.
53) S. Faujdar, and M. Agrawal, "Computational fluid dynamics based numerical study to determine the performance of triangular solar air heater duct having perforated baffles in v-down pattern mounted underneath absorber plate," *Solar Energy*, 228 235–252 (2021). doi:https://doi.org/10.1016/j.solener.2021.09.006.
54) S. Sharma, R.K. Das, and K. Kulkarni, "Computational and experimental assessment of solar air heater roughened with six different baffles," *Case Studies in Thermal Engineering*, 27 101350 (2021). doi:https://doi.org/10.1016/j.csite.2021.101350.
55) S. Sharma, R.K. Das, and K. Kulkarni, "Experimental analysis and thermal management of solar air heater roughened with sine wave baffles," *Proceedings of the Institution of Mechanical Engineers, Part A: Journal of Power and Energy*, 0 (*0*) 09576509221092906 (n.d.). doi:10.1177/09576509221092906.
56) H. Parsa, M. Saffar-Avval, and M.R. Hajmohammadi, "3D simulation and parametric optimization of a solar air heater with a novel staggered cuboid baffles," *Int J Mech Sci*, 205 (*April*) 106607 (2021). doi:10.1016/j.ijmecsci.2021.106607.
57) D. Wang, J.J. Liu, Y. Liu, Y. Wang, B. Li, and J.J. Liu, "Evaluation of the performance of an improved solar air heater with 's' shaped ribs with gap," *Solar Energy*, 195 (*13*) 89–101 (2020). doi:10.1016/j.solener.2019.11.034.
58) Bekele, M. Mishra, and S. Dutta, "Effects of delta-shaped obstacles on the thermal performance of solar air heater," *Advances in Mechanical Engineering*, (2011). doi:10.1155/2011/103502.
59) R.L. Webb, and E.R.G. Eckert, "Application of rough surfaces to heat exchanger design," *Int J Heat Mass Transf*, (1972). doi:10.1016/0017-9310(72)90095-6.